J. Fluid Mech. (2000), *vol.* 403, *pp.* 329–349. Printed in the United Kingdom

Mechanisms of transition and heat transfer in a separation bubble

By PHILIPPE R. SPALART[1]
AND MICHAEL Kh. STRELETS[2]

[1]Boeing Commercial Airplanes, P.O. Box 3707, Seattle, WA 98124, USA
[2]Federal Scientific Center 'Applied Chemistry', St. Petersburg 197198, Russia

(Received 17 February 1998 and in revised form 26 July 1999)

The laminar boundary layer on a flat surface is made to separate by way of aspiration through an opposite boundary, causing approximately a 25% deceleration. The detached shear layer transitions to turbulence, reattaches, and evolves towards a normal turbulent boundary layer. We performed the direct numerical simulation (DNS) of this flow, and believe that a precise experimental repeat is possible. The pressure distribution and the Reynolds number based on bubble length are close to those on airfoils; numerous features are in agreement with Gaster's and other experiments and correlations. At transition a large negative surge in skin friction is seen, following weak negative values and a brief contact with zero; this could be described as a turbulent re-separation. Temperature is treated as a passive scalar, first with uniform wall temperature and then with uniform wall heat flux. The transition mechanism involves the wavering of the shear layer and then Kelvin–Helmholtz vortices, which instantly become three-dimensional without pairing, but not primary Görtler vortices. The possible dependence of the DNS solution on the residual incoming disturbances, which we keep well below 0.1%, and on the presence of a 'hard' opposite boundary, are discussed. We argue that this flow, unlike the many transitional flows which hinge on a convective instability, is fully specified by just three parameters: the amount of aspiration, and the streamwise and the depth Reynolds numbers (heat transfer adds the Prandtl number). This makes comparisons meaningful, and relevant to separation bubbles on airfoils in low-disturbance environments. We obtained Reynolds-averaged Navier–Stokes (RANS) results with simple turbulence models and spontaneous transition. The agreement on skin friction, displacement thickness, and pressure is rather good, which we attribute to the simple nature of 'transition by contact' due to flow reversal. In contrast, a surge of the heat-transfer coefficient violates the Reynolds analogy, and is greatly under-predicted by the models.

1. Introduction

1.1. *Motivation*

Transition to turbulence occurs in a variety of manners. Much of the research on boundary layers has addressed transition by gradual amplification of small disturbances, such as cross-flow vortices or Tollmien–Schlichting (TS) waves, for the good reason that such cases make the location of transition most uncertain. Progress in stability methods, which are most applicable to that type of transition, should displace direct numerical simulation (DNS) transition work and steer it towards flows dominated by non-local and nonlinear effects, such as the present one.

Wings and blades with moderate Reynolds numbers and low sweep angles often cause their boundary layer to separate while still laminar; the detached shear layer may become turbulent rapidly enough to achieve reattachment on the surface, creating a 'short bubble' (airfoil chord Reynolds numbers below about 70 000, Lissaman 1983). This is well known in classical aerodynamics, and revealed by a 'flat spot' on the pressure distribution as the bubble alters the effective shape of the airfoil (Gaster 1966). It appears that transition is inevitable, except at the smallest Reynolds numbers, but the length of the bubble depends on the development of the turbulence. This is of importance for high-lift devices on aircraft, particularly in wind-tunnel tests, and in gas turbines. Some high-performance low-Reynolds-number airfoils include a short bubble by design, providing a 'transition ramp' to foster instabilities and precipitate transition (Liebeck 1978).

As the reach of computational fluid dynamics rapidly approaches complex three-dimensional separated flows, turbulence models should be submitted to tests on separation bubbles. In our studies of this classical subject, DNS has much potential to complement experiments in the exploration of the mechanisms that cause transition. In quantitative comparisons, for instance when testing turbulence models, DNS has the advantages of freedom from sidewall problems, strictly two-dimensional mean flow (if desired), and complete information on the flow field. Its principal disadvantages are cost and limitations on geometry and Reynolds number.

The wall heat transfer in separation bubbles (even fully turbulent) appears to break the usual Reynolds analogy with momentum transfer (Spalart & Coleman 1997) which makes skin-friction measurements particularly difficult and appears to create an additional challenge in turbulence modelling. It is trivial for the analogy to fail when the skin friction crosses zero, but we also have interest in the recovery region, and later in three-dimensional flows, for which separation does not imply a zero skin-friction vector. Heat transfer is furthermore used to detect transition in experiments. Finally, the turbine blades in turbo-machines are very sensitive to heat transfer, have low sweep, and moderate Reynolds numbers (on the other hand, they are exposed to high free-stream turbulence levels, causing another type of 'by-pass' transition which we are not considering here). This motivated us to include temperature as a passive scalar in an incompressible flow. Our first publication had only one scalar with an isothermal wall, which is numerically easier (Spalart & Strelets 1997); we now also address heat transfer with uniform wall flux, which is more realistic both in actual systems and when the heat transfer is controlled for fundamental studies, for instance by Vogel & Eaton (1985) and Rivir, Johnston & Eaton (1994). This second temperature field is not as mature as the first one, because it was included only in the latter part of the simulation, but is mature enough to deserve analysis and buttress the findings made on the first field.

1.2. *Design*

We set out to create a transitional separation bubble under the simplest conditions, easy to reproduce numerically if not experimentally. They are nearly identical to those of Pauley, Moin, & Reynolds (1990). Very few of the separation experiments provide the ceiling shapes and aspiration/blowing rates needed to calculate the flows. Airfoil experiments (Crouch & Saric 1986) do, but they have less detail and are less attractive for DNS because of size and surface curvature. We note that Gaster (1966) also studied bubbles on a straight wall. A transitional bubble is more physically interesting than a fully-turbulent one (such as Spalart & Colesman 1997) and achieves reattachment more promptly even in an adverse pressure gradient. This

slightly relieves the need for high Reynolds numbers, which is helpful in a DNS. We speculate that this flow transitions by what we loosely call an absolute instability (Huerre & Monkewitz 1985), as opposed to the convective instability of TS waves, and that we have a global transition mechanism, in the sense that the turbulence inception depends on the flow farther downstream in the bubble. The expectation is of a dominant Kelvin–Helmholtz instability, in view of the marked inflection point in the velocity profiles after separation. The initial three-dimensionality is also of much interest, in that we could envision a secondary instability as happens with TS waves in Blasius flow, or a primary instability such as Görtler vortices.

We made the fundamental choice of eliminating incoming disturbances in the entry region of the boundary layer, as far as possible, instead of introducing and varying them (controlled intentional disturbances are the only choice when studying convective instabilities such as in the Blasius boundary layer, but some groups firmly favour that approach even in separation bubbles). Again, our choice was also Gaster's (1966) and Horton's (1967): they argued that once they are low enough, incoming disturbances are dominated by the effects of pressure gradient and separation. In order to deserve recognition, the DNS needs to have a very low level of disturbances in the entry region and to be accurate, while having a high enough Reynolds number to create viable turbulence. We believe we reached this objective, by sustaining the pressure gradient long enough, without incurring a computing cost out of line with current DNS projects. We are offering the electronic dataset to colleagues wishing to test their turbulence models (Hadzic & Hanjalić 1999).

It also appeared that, unlike transition by gradual amplification under a quiet free stream, this kind of transition could well be amenable to Reynolds-averaged calculations, even with simple models. By this we mean models in their standard form, without any devices added to accurately duplicate transition. Our reasoning is that such devices contain valuable information and help in fairly simple flows, typically two-dimensional flows amenable to boundary-layer calculations, but are not and cannot easily be incorporated into the current generation of three-dimensional Navier–Stokes codes and turbulence models, which we strive to make applicable to any geometry (these devices also use outside information such as the knowledge of the transition point, and inconvenient quantities such as the boundary-layer thickness). In a RANS solution using a transport-equation turbulence model, the regions with non-zero turbulence-model quantities expand, which is a form of entrainment. When such a region touches a shear layer which has remained laminar, that layer quickly becomes turbulent. This may be crude (in reality, transition can be greatly accelerated even without actual contact of the shear layers), but it is qualitatively correct, and we call it 'transition by contact'. In the separation bubble, it is the return flow which brings turbulent fluid into contact with laminar fluid. We believe transition of transport-equation turbulence models by contact should be studied further; given a little attention, it happens spontaneously in complex calculations when users allow laminar regions. We had evidence that laminar separation can be followed by transition, but not that the rate at which transition occurs is accurate (although the 'trip-less' results of Shur *et al.* (1996) were indeed better than fully-turbulent results, for a circular cylinder in the plausible Reynolds-number range for laminar separation). This led us to run RANS cases along with the DNS.

This flow may be labelled as a 'by-pass transition', in the sense that a protracted amplification does not take place, but there is no suggestion that by-pass transitions in different situations, such as at the tip of cones or under high free-stream turbulence,

share a common mechanism. The term by-pass has also been mis-used, for instance when referring to turbulent attachment lines on swept wings.

Much effort has been directed at the theory, experiment and DNS of separation bubbles with a different slant from ours, notably in Germany and Russia (Dovgal, Koslov & Michalke 1994; Maucher, Rist & Wagner 1999). Waves are input upstream, usually small and with a simple spectrum, two-dimensional and oblique. The focus is on the growth of these disturbances across the bubble, and the bubble is often small enough for a laminar reattachment to occur. These studies should lead to a rigorous description of the modes involved, but after a much more lengthy process than our direct search for the natural modes which exist in a full nonlinear solution, with a deceleration extensive enough that the pressure gradient returns to adverse after transition (as it does in practice).

Transition in similar conditions was studied using DNS by Alam & Sandham (1997*a*, *b*) and using large-eddy simulation (LES) by Wilson & Pauley (1995) and Yang & Voke (1995). Alam & Sandham and Wilson & Pauley used a flat plate and aspiration as we do, whereas Yang & Voke used a somewhat more realistic, and numerically more difficult, semi-circular leading edge. Wilson & Pauley duplicated the 'inviscid pressure distribution' of Gaster (1966), but not his geometry. We did not attempt this, partly because the geometry difference becomes more relevant once separation takes place, and partly because we assumed (erroneously) that his Reynolds number would be out of reach of DNS. The LES technique appears less attractive to us than the DNS technique because major intervention has often proven necessary in the subgrid-scale model to correctly duplicate transitional behaviour (Yang & Voke 1995 switch manually between two values of the Smagorinsky constant). We have also seen this in channels and attached boundary layers. The newer 'dynamic' subgrid-scale models appear to be more autonomous and to 'light up' automatically, while still requiring disappointing emergency measures such as averaging in the spanwise direction (Wilson & Pauley 1995). Thus, an essential ingredient of such simulations is non-universal; the ability of LES to carry over from one type of flow to the next appears to be in question. Over the years, LES of transitional flows may mature, possibly thanks to dynamic models, and rival the more expensive DNS approach we used here. However, today, DNS appears much more appropriate for the 'free-standing' study of a flow, without experimental support.

The three other DNS studies and this one have similar Reynolds numbers. We used nearly an order of magnitude more grid points and were consequently limited to a single case, although with two scalar fields, and to a modest time sample. Our Fourier series in the streamwise direction also preclude grid stretching, which would allow a better use of these grid points. A physical difference relative to the leading-edge flow of Yang & Voke is the absence of the receptivity mechanism associated with the step in surface curvature. Relative to Wilson & Pauley (1995), we elected not to stimulate Görtler vortices; such vortices do *not* show up naturally in our DNS.

The simulation of Alam & Sandham (1997*b*) is most comparable to the present one. Their Reynolds number at separation is comparable, but the bubble is shorter. The deceleration is less, but it is more abrupt. More importantly they imposed disturbances, oblique waves, with a 'disturbance strip'. We are quite confident that their flow would 'hold' transition without those, just like ours, at least if they were to increase their deceleration beyond 20%.

In this paper, § 2 defines the problem of fluid mechanics we are treating; § 3 outlines the numerical methods; § 4 contains results and § 5 a discussion.

2. Specification of the flow

The boundary conditions are nearly identical to those of Pauley *et al.* (1990), except of course for the third dimension which we take periodic as in Wilson & Pauley (1995), Spalart & Coleman (1997), and many others. A viscous wall at $y = 0$ creates the boundary layer, and an 'inviscid' boundary at $y = Y$ controls the pressure gradient. The depth Y will be used to normalize lengths. At the inviscid boundary, the boundary condition in the streamwise velocity u is no stress ($u_y = 0$) for Pauley *et al.* (1990), but zero vorticity ($u_y = v_x$) here. This has little importance, since fluid only leaves the domain through this boundary; the vorticity difference is convected out of the domain. Neither condition requires a fine grid at the upper boundary, which allows the numerical method in the y-direction to be tangibly more economical than the Chebyshev methods that are sometimes used. An aspiration velocity $V(x)$ at Y is specified (that is, $v(x, Y, z, t) = V(x)$), which is non-zero only in the vicinity of a 'slot' centred at $x = X$. These conditions can be closely duplicated in an experiment (provided sidewall problems are solved), unlike those we used for a turbulent bubble (Spalart & Coleman 1997 had aspiration followed by blowing, so that the vorticity of the re-injected fluid would matter). If U_0 is the velocity upstream in the channel, the nominal deceleration is measured by the ratio

$$S \equiv \frac{1}{Y U_0} \int V(x)\, \mathrm{d}x$$

using Pauley's notation. If the non-zero region of the V-distribution in the x-direction is narrow enough, compared with Y, the boundary layer is sensitive only to the above integral (we used a Gaussian distribution $\exp(-[(x - X)/(0.24Y)]^2)$). We verified this in RANS cases. If the inflow and outflow boundaries are far enough away not to matter, the boundary conditions are reduced to three non-dimensional parameters: S; the depth Reynolds number $R_Y \equiv Y U_0/\nu$; and the streamwise Reynolds number $R_X \equiv X U_0/\nu$. Here, X is measured from the virtual origin of the incoming Blasius boundary layer, and ν is the viscosity. To have a thin boundary layer in the entry region, we require $\sqrt{R_X} \ll R_Y$. Heat transfer adds another parameter, the Prandtl number Pr which we set to 0.71, and the type of wall condition. For the first temperature field, t_1, it is isothermal. The temperature is uniform near the upper boundary, of course.

The procedure for the second field t_2 is not as simple, but is more realistic. We established by iteration a distribution of temperature at the wall, $t_2(x)$, which results in a uniform *mean* wall heat transfer: $\partial^2 T_2/\partial x \partial y = 0$. We use the notation T_2 and t_2' for the mean and root-mean-square temperatures; averages are taken in z and t, leaving them functions of (x, y). Thus, t_2 also obeys a Dirichlet boundary condition, but non-uniform in x; such conditions are commonly used for stability studies (the mean flow obeys a Neumann condition, but the perturbation obeys a Dirichlet condition). The wall temperature is implicitly given in a later figure, which shows the heat-transfer rate, normalized by the temperature difference $T_2(x, \infty) - T_2(x, 0)$. The raw heat transfer was not exactly uniform, as brief excursions of $\pm 10\%$ remained after iterating. This procedure is close to a physical situation in which the wall material has thermal inertia and a uniform heat source or sink behind it. In the RANS, there was no issue; the model made the turbulent heat flux zero at the wall (consistent with $t_2' = 0$), and a Neumann condition applied to T_2, thus setting the molecular heat flux. Turbulence models of high enough order would distinguish between the condition we applied and an instantaneous Neumann condition.

Pauley *et al.* (1990) presented two-dimensional results for S in the range $[0.09, 0.22]$, R_X in the range $[6 \times 10^4, 24 \times 10^4]$, and $R_Y \approx R_X/5$. They obtained periodic vortex shedding in two-dimensional solutions. We also find the threshold for flow reversal and shedding to be near $S = 0.12$ for their Reynolds numbers, but it is very grid sensitive. For the transitional case we chose $S = 0.3$, $R_X = 10^5$, $R_Y = R_X/3$, in order to produce a large enough bubble and a fairly high Reynolds number. For a given S and R_X, a larger R_Y makes the pressure rise more gradual. For a Blasius region to exist before the pressure rise, which we require to enable meaningful comparisons, R_Y must be less than about half of R_X.

In an experiment, boundary-layer fluid may need to be removed upstream of the test region to obtain the correct virtual origin. The facility would have to match R_X and R_Y, making it rather shallow; an insert in a wind tunnel may be best. If the boundary-layer thickness before removal is fairly small compared with Y, we do not expect it would have much influence at all. However, we are not ready to predict how low a disturbance level could be obtained, and venture that sustained or repeated suction may be desirable if the boundary layer starts turbulent. Certainly, measurements would be made to confirm Blasius behaviour and low disturbance levels in the entry region.

3. Calculation methods

The DNS code is close to that of Spalart & Coleman (1997). It is spectral in space and mixed third/second order in time. The inflow and outflow are treated by the fringe method (Spalart 1988*a*), with additional wall-suction and damping terms to suppress disturbances in the fringe, similar to our other transition studies (Bertolotti, Herbert & Spalart 1992). The resolution is at least as fine as that proven in fully turbulent boundary layers (Spalart 1988*b*), in wall units based on the peak friction velocity, $u_\tau \simeq 0.038 U_0$. This flow is more demanding, since we require very low disturbance levels upstream. The grid was refined beyond the usual turbulence values in the x- and y-directions, based on observations of the spurious fluctuations in the irrotational region. These are never exactly zero, and originate in numerical oscillations. Normalized with Y, the grid spacing is 0.0094 in the x-direction with about 800 points in the useful region (200 in the fringe); 0.005 in z with 120 points; and variable in y with about 100 points out of 120 within the boundary layer at its thickest ($\delta \simeq 0.5$). The spanwise period equals 0.6, which is about 7 times the displacement thickness at the outflow (as opposed to a ratio of 25 in Spalart 1988*b*), or 8 times the total thickness of the detached laminar shear layer.

The initial condition of the DNS contained three-dimensional random perturbations; their details and level are not relevant in the developed solution. The approach to steady state was verified in the integral quantities, and established based on the temperature-deficit equilibrium, shown in §4.2. The fringe terms and slot location were adjusted to provide a Blasius entry region with the desired distance, namely 3, between the virtual origin and the slot centre. The outflow conditions are not critical, as shown by the smoothness of the curves in this and other fringe simulations.

The RANS solver uses the upwind-difference scheme of Rogers & Kwak (1990). This is an implicit flux-difference splitting scheme of third-order accuracy for the convective terms, and second order for the viscous terms. The method is implemented by line Gauss–Seidel relaxation. The S-A eddy-viscosity transport equation (Spalart & Allmaras 1994) is solved jointly with the RANS equations with first-order accuracy for the convective terms; limited results will be shown for other models, which were

treated in a similar manner. A non-uniform grid (with clustering in the vicinity of the wall and aspiration region) is used with the total number of grid points 201×101. The spacing in x is between 0.03 and 0.05. The maximum value of the normalized near-wall grid spacing, Δy^+, in the turbulent region is no higher than 0.6. The ratio of neighbouring steps is less than 1.05 for x, and less than 1.2 for y. Grid studies give error estimates below 5% for quantitites such as the skin-friction peak, which is among the more sensitive indicators. Specifically, the peak increased by 3.5% when going from 151×77 to 201×101 and 2.8% from 201×101 to 261×131. Runs with first-order and with second-order differencing (but still upwind) for the model transport equation also revealed negligible differences. The constants c_{t3} and c_{t4} of the S-A model were varied. These are arbitrary to some extent, and have control over spontaneous transition when it is caused by noisy numerical solutions. We conjectured that they might influence transition here, but found that they had no effect.

The RANS solution uses the 'Trip-Less' approach of Shur *et al.* (1996); the eddy viscosity is zero (or at least negligible compared with the molecular viscosity) in the entry region and transition (eddy-viscosity growth) occurs only because reverse flow carries non-zero values upstream in the bubble. This was achieved by setting non-zero inflow values during the first iterations, and then setting zero inflow values until a new steady state was reached. Thus, we did elect to activate the turbulence model, which can be viewed as a 'time trip', but the transition location in the converged solution is fully controlled by the permanent boundary conditions, as opposed to the initial conditions. Were the flow attached, all turbulence would be evacuated downstream. The two-dimensional RANS solution has a stable steady state, unlike two-dimensional solutions without turbulence model, such as those of Pauley *et al.* (1990). The trip-less RANS solution appears to be unique. Uniqueness is never certain with a large system of nonlinear equations, but runs with different grids or initial conditions (other than laminar) led to the same solution.

4. Results

4.1. *Visualization of the DNS*

Figure 1 aims at an understanding of the proportions of the flow and its character in the different regions. It shows contours of the vorticity magnitude and of the first scalar, t_1; the second scalar is highly correlated with the first one. The contours on the wall are of the derivatives $\partial u/\partial y$ and $\partial t_1/\partial y$; they are strongly correlated. From here on, lengths are normalized with Y and velocities with U_0. The DNS fringes leave a 'useful region' that covers roughly $[0.5, 7.5]$ in the x-direction. The interval shown for the streamwise direction in figure 1 is $x \in [2.5, 7]$; recall that the ceiling aspiration slot is at $x = 3$ and mean separation around 2.25.

Starting from the left, we first see a very smooth separated vorticity layer, with negligible z dependence. Superimposed on it is a layer that carries a steep scalar gradient. Quite suddenly near $x = 3.5$, intense fine-scale vorticity appears. The scalar shows more 'precursor' three-dimensionality under the gradient layer, although the relative contour levels are arbitrary. The region with non-zero vorticity and that with non-free-stream scalar values are closely matched and exhibit strikingly deep 'valleys' in the turbulent part of the flow. Those of Alam & Sandham (1997*b*) were not as deep. Intermittency almost reaches the wall; much 'engulfment' of irrotational fluid takes place. This is not inconsistent with experimental flow visualizations (see the picture by Corke, Guezennec & Nagib in Van Dyke 1982, p. 92). This 'marked region' also shows that the spanwise coherence of the flow is destroyed. Note also how the

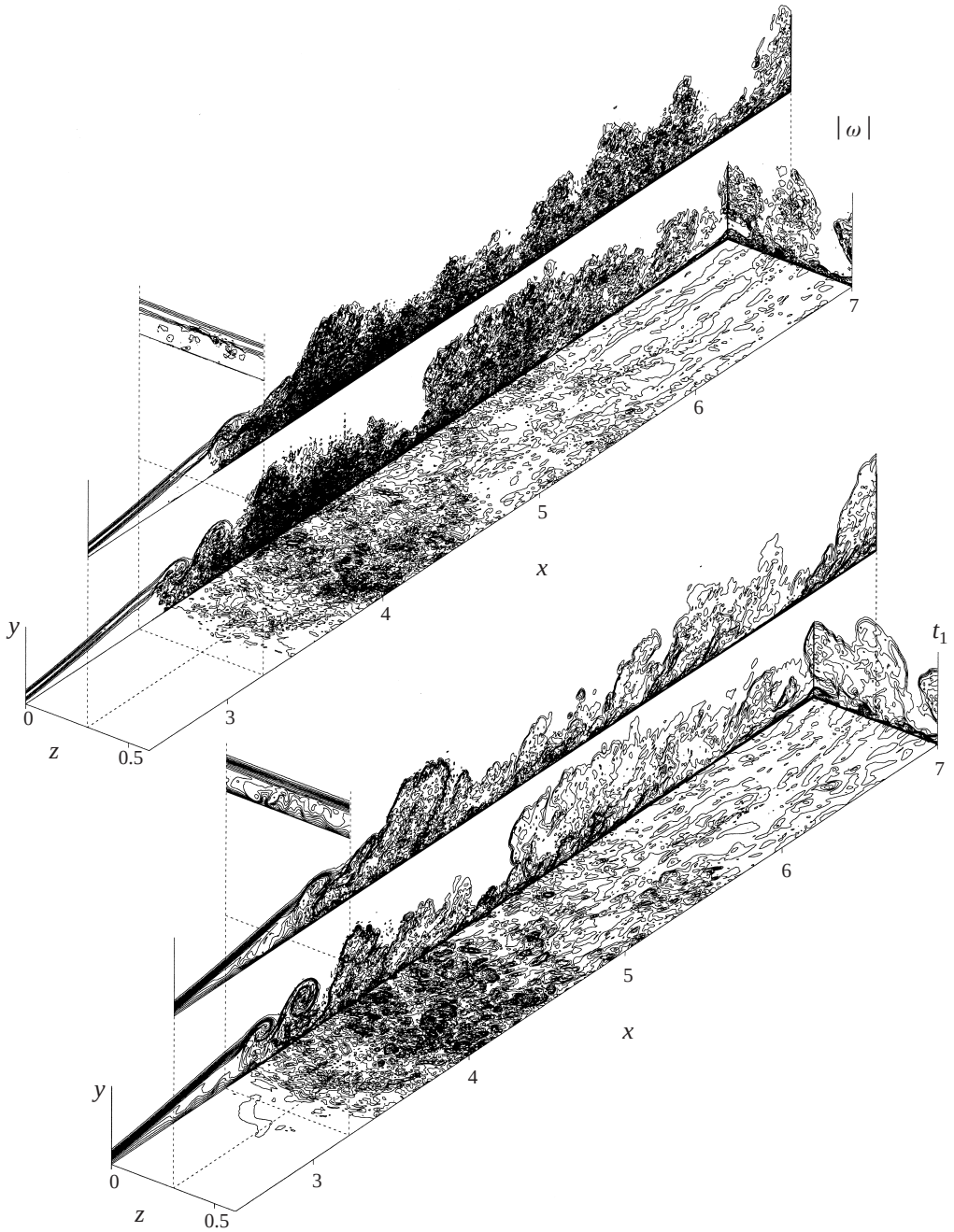

FIGURE 1. Visualization of the vorticity and temperature in the DNS. The fringes end at $x \simeq 0.5$ and start again at $x \simeq 7.5$. Mean separation is at $x = 2.25$ and mean reattachment at $x = 4.25$.

wall contours are fairly isotropic at transition. Subsequently, the variations become less intense, and elongated streamwise; the usual near-wall 'streaks' are appearing. Shear and scalar gradient are again correlated. The 'Lambda' vortices so familiar in transitioning attached boundary layers are not seen.

This figure is quite satisfactory in the sense that, in spite of the large range of scales

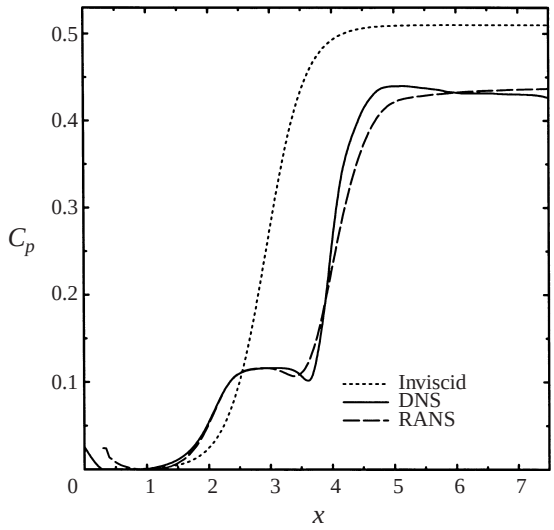

FIGURE 2. Wall pressure coefficient.

for the vorticity and the scalar gradient, no numerically-induced oscillations are in evidence in either part. We detected, however, small regions in which t_1 is outside the interval [0, 1]. These are clearly of numerical origin, because the initial condition was in that interval everywhere, and the exact scalar transport equation cannot create new extrema. The excursions measure up to about 1.07, and are all located on the downstream side of large turbulent bulges with sharp interfaces, symptoms of localized Gibbs phenomena (oscillations caused by the inability of the discretization to fully resolve the steepest gradients) in the x-direction. This is a reminder that no numerical solution is ever exact; however, such scrutiny has not been reported in other DNS or LES studies of similar flows.

4.2. *Integral quantities*

We present pressure coefficients in figure 2. By 'inviscid wall pressure', in the figure, we mean the pressure that would exist with a slip condition on the lower wall and therefore irrotational flow. It has a smooth rise from $C_p = 0$ to $C_p = S(2 - S)$, symmetric with respect to the slot at $x = 3$ (to be precise, it is $\sqrt{1 - C_p}$ which is symmetric, not C_p). The viscous C_p reaches only about 0.43, instead of 0.51, because the displacement thickness is near 0.08 downstream of the bubble, which lessens the deceleration from 30% to about 25%. The displacement effect at the bubble itself creates the expected flat spot on the pressure, followed by a rapid rise. Note also the anticipated rise near $x = 2$, caused by the concave curvature of the streamlines. This was observed in experiments, by comparing with a tripped case, which remained attached and therefore close to the inviscid C_p (Gaster 1966). The values of the two dominant parameters in Gaster's correlation are the Reynolds number at separation $R_{\theta s} \simeq 180$ and the deceleration $P \simeq -0.1$. This puts the flow in the region of bubbles without 'bursting' according to Gaster, therefore a prompt reattachment was to be expected. The comparison with airfoil experiments (Gaster 1966; Horton 1967) is a little obscured by the fact that the wall pressure does not return to the inviscid curve, as seen in figure 1. This is due to the proximity of the opposite boundary. The agreement between DNS and RANS is better than expected, considering that the turbulence models were calibrated exclusively using fully turbulent, and thin, shear flows.

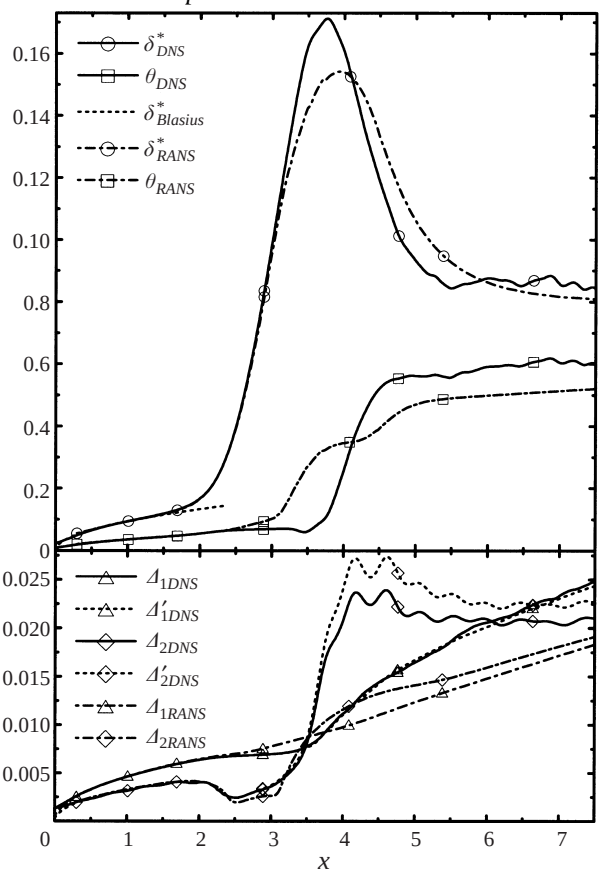

FIGURE 3. Boundary-layer thicknesses.

We present thicknesses in figure 3. In the definition of the velocity thicknesses δ^* and θ, the velocity U is ill-behaved outside the viscous region, because of curvature ($U_y = V_x \neq 0$), and is replaced by the pseudo-velocity $\overline{U}(x,y) \equiv -\int_0^y \omega_z(x,y')\,\mathrm{d}y'$ (this procedure is helpful here, but unfortunately not in compressible flows). On the other hand, the true velocity is used in the temperature-deficit thickness $\Delta \equiv \int_0^Y U(T_\infty - T)\,\mathrm{d}y/(T_\infty - T_w)$, T being well-behaved. Here, $T_w(x)$ is the wall temperature and T_∞ the free-stream temperature. Δ is very valuable as a check of equilibrium, with no need for boundary-layer assumptions (we have failed to find a similar integral equation for momentum conservation). The quantity Δ' is the right-hand side of the integrated temperature equation; at equilibrium, $\Delta = \Delta'$. Both Δ and Δ' are normalized by the temperature difference:

$$\Delta' \equiv \frac{1}{T_\infty - T_w}\left[\int_0^\infty \left[\overline{u't'} - \frac{1}{Re\,Pr}\frac{\partial T}{\partial x}\right]\mathrm{d}y + \frac{1}{Re\,Pr}\int^x \frac{\partial T}{\partial y}_{y=0}\,\mathrm{d}x' + \Delta_0\right]$$

where the constant Δ_0 (or equivalently the lower bound of the second integral) is set to make Δ and Δ' coincide at a value of x within the laminar region.

The figure allows several checks. The temperature thicknesses Δ and Δ' match well for the first DNS scalar, which benefits from a time sample of about 18 (again normalized with Y and U_0). The velocity field has the same sample, suggesting at least as good a match for momentum balance. In contrast, the second scalar matches

well only to $x \simeq 3.6$, in the transition region. Subsequently, the curves are not very close and inherit some waviness from T_w. This scalar field was started much later, and its time sample is only about 6. The close agreement in the laminar region indicates correct programming of the second boundary condition; the sample is too short for definitive values in the turbulent region, but not to challenge turbulence models with the second boundary condition. The figure also shows agreement with the Blasius distribution for δ^*, another check on both numerical methods. The shape factor $H \equiv \delta^*/\theta$ at reattachment is 3.1, in fair agreement with Horton's compilation, which gave 3.5. Horton's criterion at reattachment $\Lambda_R \equiv [(\theta/u_e)\mathrm{d}u_e/\mathrm{d}x]_R$ takes the approximate value -0.009, when he recommended -0.0082. Horton (1967) also indicated that the Reynolds number based on the length of the laminar separated layer and the edge velocity is 40 000; we find about 36 500. Thus, several classical compilations are corroborated. The DNS is at a 'full-scale' Reynolds number.

We now use the figure to compare DNS and RANS results. They agree quite well on δ^*, which is consistent with the pressure (figure 2). However, θ rises earlier in the RANS, and the thicknesses are 10% to 15% too low downstream in the RANS. The temperature thicknesses are much more troublesome, as the discrepancies already appear near $x = 2.5$, not unlike the momentum thickness, and become very serious by $x \simeq 4$. The RANS duplicates the peculiar drop in Δ_2 after separation, due to the widening temperature difference $(T_\infty - T_w)$, but fails to follow the steep rise after transition. It will, clearly, take some distance to recover from this discrepancy.

The wall-transfer coefficients in figure 4 are sensitive, and exhibit appreciable modelling inaccuracies. Slight differences are seen in the laminar region; detail differences in the treatment of the inflow boundary induce weak residual pressure gradients, as seen in figure 2. Both sets of results have a negative surge of skin friction around $x = 3.8$, which we did not foresee but is justified by the steep pressure rise, following a region with essentially zero values. The same surge was seen by Alam & Sandham (1997*b*). The phenomenon is not as marked as in the experiment of Dianat & Castro (1991). Their boundary layer, first turbulent and relaminarized, produced sizeable positive values of skin friction before entering a long region with negative values.

The recovery to positive skin-friction values is too slow with RANS, missing even the local maximum near $x = 5$. We did not expect this, as models often approach 'standard' states faster than they should, but it has become a pattern for many reattaching flows (Menter 1994*b*). At $x = 7.5$, the DNS gives $R_\theta \simeq 1500$, $C_f' \simeq 0.0044$ (both based on the local edge velocity $\overline{U}(x, \infty)$ rather than on U_0), and $H \equiv \delta^*/\theta \simeq 1.41$. These values are not far from normal in zero pressure gradient, as we would expect $C_f' \simeq 0.0039$, $H \simeq 1.44$. The RANS gives $R_\theta \simeq 1300$, $C_f' \simeq 0.0035$, $H \simeq 1.55$ (at $x = 7.5$, δ^* is still dropping, so that even the briefest examination of the thicknesses reveals the incomplete development). A longer recovery region would be desirable, but $R_\theta \simeq 1500$ is not far from the current limit of DNS. The Blasius curve for C_f is also shown.

The Stanton numbers are even more challenging, as foretold by the temperature thicknesses. The RANS completely misses the large surges at transition, which would of course be quite a concern in gas-turbine applications. Recall that the S-A model simply uses a constant turbulent Prandtl number equal to 0.9 (limited tests with a lower turbulent Prandtl number in the upper region failed to provide much improvement). The agreement improves downstream. Notice how mismatched the momentum and temperature boundary layers are in that region: Δ is less than half of θ, whereas in a simple boundary layer (and in a laminar layer) it would be a little larger. Correlatively, $2St'$ is near 0.0071, which far exceeds C_f; as a result the gap between Δ and θ will slowly close, further downstream.

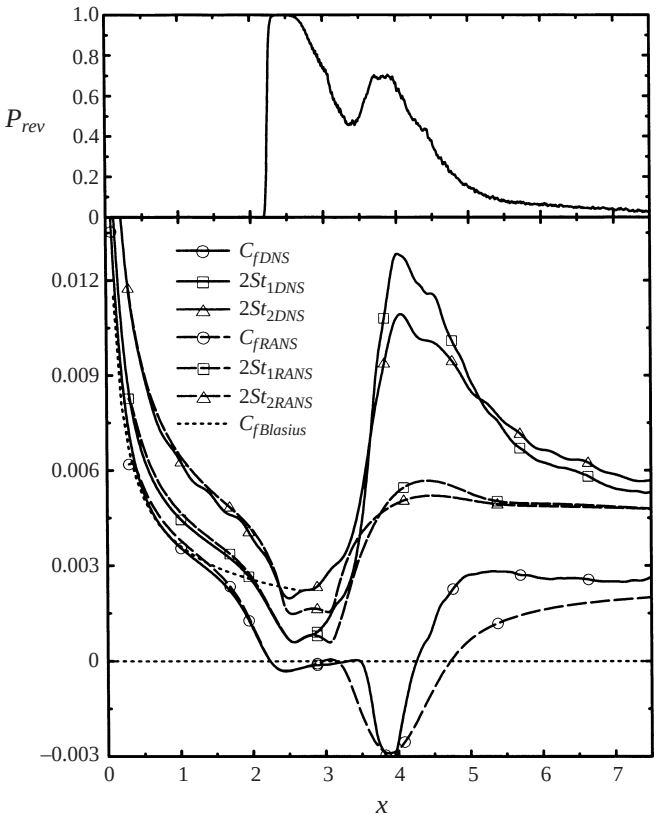

FIGURE 4. Wall transfer coefficients, based on U_0 and $T_\infty - T_w$, and probability of reverse wall shear (upper graph).

The upper graph of figure 4 shows the probability P_{rev} for the wall shear stress to be negative. It jumps from 0 to 1 near $x = 2.25$, revealing the very weak dependence on time and on the spanwise coordinate (figure 1). In the turbulent part of the bubble, it is quite far below 1, much like in bubbles with turbulent entry (Alving & Fernholz 1996; Spalart & Coleman 1997). It then decays, but quite slowly as a result of elevated turbulence levels relative to the mean skin friction, and is still non-zero at $x = 7.5$. Alam & Sandham (1997*b*), in contrast, arrive at 'a stage where all the flow is attached'. In fact, a visualization of our solution such as figure 1 but limited to negative contours shows that these regions are very sparse beyond $x = 5$.

Figure 5 shows the skin-friction coefficients with other turbulence models, all based on simple transport equations (Shur *et al.* 1995; Menter 1994*a*). The SST model of Menter was run both in its original form and with a term derived from the 'f_{t2}' term of the S-A model, which prevents premature (numerical) transition. Without that term, the SST model gives early transition, and no separation. Both the slightly modified SST model and the v_t92 model of Secundov give transition a little earlier than S-A, and quite a bit earlier than the DNS. Conversely, their skin friction is noticeably more accurate than S-A in the recovery region. Finally, their pressure coefficient C_p after relaxation is near 0.46, which is less accurate than S-A. Based on this single case, there is little to choose between the three models. The results are quite encouraging for such simple transport-equation models. However, few models accept zero values

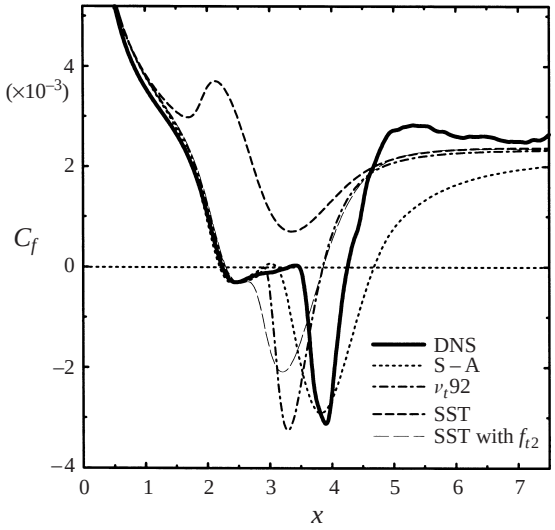

FIGURE 5. Skin-friction coefficients.

in the laminar regions, and a behaviour after separation that is both sensible and insensitive to inflow values cannot be counted upon in general.

4.3. *Transition mechanism*

The results here all come from the DNS. Figure 6 shows the peak values of u', w', t'_1, and t'_2 within the boundary layer. All but t'_2 are well below 0.1% in the Blasius region, indicating that the damping of the turbulence through the fringe was quite effective. Typical levels outside the boundary layer are 0.03%. However, some authors report effects on bubble length at least down to 0.2% (Mayle 1991), so that it is difficult to guarantee that residual fluctuations play no role. At separation, $x \simeq 2.25$, w' increases by a factor of 50, indicating a dramatic rise of the three-dimensionality. The peaks of u' and t' then smoothly rise to near 10% at $x = 3.5$, with w' lagging. The u' level peaks around 23%; this is in only moderately good agreement with Gaster's 16%, but the exact normalization is not unique. After transition, the peak u' in wall units decays from about 3.7 at $x = 5$ to the usual 2.7 at $x = 7.5$. However, a normal log layer is not established; U^+ at $y^+ = 100$ is less than 15, when the accepted bracket is [16.2, 16.7]. Other workers have also found the wall-unit velocity profiles to be lower than normal even far downstream of reattachment, in fact, much farther than our DNS covers (Alam & Sandham 1997*b*; Castro & Epik 1996).

The levels of t'_2 upstream of transition are much higher than the other ones, of the order of 1% normalized by the temperature difference, because that field is not as well converged. It reflects a residual time dependence, not a spanwise dependence. We have no evidence that it is due to the different boundary condition.

The growth rate $\mathrm{d}(\log u')/\mathrm{d}x$ upstream of transition rises from about 1 to 4, then comes down to 2. Growth is steep even upstream of $x = 1$, where the Blasius boundary layer is stable to TS waves (the Reynolds number based on δ^* is 314). The instantaneous side views in figure 1 show a sudden change from a very smooth shear layer to a rolled-up vortex, with small-scale activity throughout the layer. See a visualization by Head in Van Dyke (1982, p. 91). Michalke (1965) points out that the mixing-layer instability, with a ratio $R \equiv |U_2 - U_1|/(U_1 + U_2)$ equal to 1, grows by a factor of 35 in one wavelength, a spatial growth rate of about 11 here (U_1 and U_2

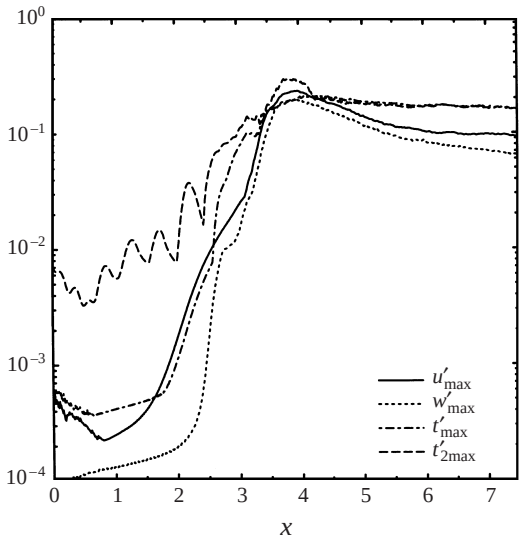

FIGURE 6. Peak r.m.s. across the boundary layer.

being the velocities on either side of the layer). These numbers apply to an unconfined mixing layer, of course. Here, R is about 1.06, giving an even larger growth ratio, so that the convective instability comes close to explaining the very sudden appearance, visually, of rolls. The absolute-instability concept of Huerre & Monkewitz (1985) may not add much to Michalke's, particularly since the R ratio does not reach their critical value ($R = 1.315$) until $x \simeq 3.63$, well into the transition region. Similarly, Alam & Sandham (1997*a*) ran a stability study of velocity profiles representative of laminar separation bubbles. They found that the reverse flow had to reach about 15% of the edge velocity before an absolute instability existed; this condition is far from being fulfilled by our profiles in the region where transition is beginning (as will be seen shortly). The present shear layer has a vorticity thickness $\delta_\omega \equiv |U_2 - U_1|/\omega_{\max}$ of about 0.045, and Michalke's analysis would predict a wavelength of about 0.3; this agrees with figure 1, which gives about 0.32. The Reynolds number $|U_2 - U_1|\delta_\omega/\nu$ is about 1500; therefore, viscous effects are likely much weaker than wall-proximity effects.

It appears that the Kelvin–Helmholtz instability is involved, but the possible dependence of the DNS results on incoming disturbances is difficult to establish beyond any doubt. Numerical errors are of course never zero and do propagate upstream, at least with the low numerical dissipation of a spectral method. However, they are dominated by very short waves, with typical wavelengths of a few grid spacings, say about 0.05 here. Thus, they are not likely to foster the wavelength 0.3. Similarly, the dominant period in time represents about 500 time steps, which rules out serious integration errors at that frequency. The 'hard' ceiling (prescribed normal velocity V) at a height of $y = 1$ reflects pressure signals, but appears much too distant to dictate the wavelength 0.3. Of course, the reflection preserves the frequency, and the base flow undergoes noticeable changes (such as 0.05 in C_p) on the scale of 0.3 in x. Such non-uniformities create a receptivity mechanism; it is physical, not numerical. Reflections from the inflow boundary are of course not zero, but that boundary is not hard (it is not a Dirichlet condition), and the very low disturbance level for $x \leqslant 1$ suggests that they play no role (the fringe ends near $x = 0.22$, u' decays smoothly from there to near 0.8).

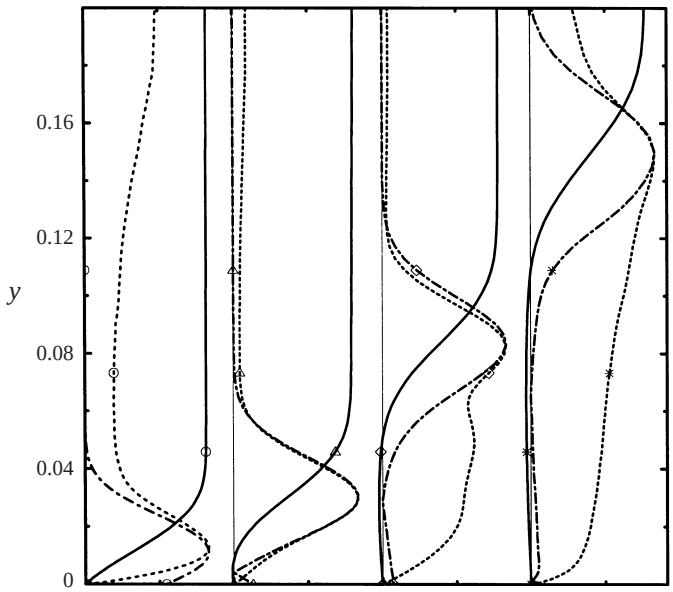

FIGURE 7. Profiles in DNS. —, U; - - -, $u'/u'_{\max}$; - — -, $|U_y|/U_{y\max}$. ○, $x = 2$; △, $x = 2.5$; ◇, $x = 3$; *, $x = 3.5$. Each profile is displaced by 1.2.

In figure 7 we show the profiles which underlie the transition. The mean velocity only reaches very small negative values, which is consistent with the small skin friction for $x < 3.5$, and clear in Gaster's figure 6. This is the 'dead-water' region. Crouch & Saric (1986) had larger values, of the order of -0.1. The profiles of u' and $|\partial U/\partial y|$, each normalized by its local maximum, are instructive. The u' profiles do not have the double-peak pattern of TS waves. Instead we have a 'wavering' shear layer (some authors use the word 'flapping'). We define a wavering shear layer as having a dependence of the type $u(x, y, z, t) = \tilde{u}(x; y - \tilde{y})$ where $\tilde{y}(x, z, t)$ is a statistical variable with small variations (compared with the layer thickness). For such a dependence, the r.m.s. of u at a fixed x is proportional to the slope of U: $u' \propto |U_y|$; typically, their common shape has a single peak. This behaviour is clear in figure 7 (see also Gaster 1966, figure 10). At $x = 2$, the shear layer does not yet have pure wavering behaviour. At $x = 2.5$, the shapes match very well except close to the wall. At $x = 3$ and $x = 3.5$, 'true' turbulence near the wall is growing, but the outer part still exhibits wavering behaviour. We see that the growth rates in the [2,4] range for $x < 3.5$ (figure 6) apply to the wavering motion (which sets the u' peak), not to the Kelvin–Helmholtz waves which eventually cause transition.

Figure 8 shows the 'waver amplitudes' $\tilde{y}'$, first deduced from u as the ratio of the peak value of u' to the value of $|U_y|$ at that same location, and then deduced from t_1 by the same formula at the same location. The amplitudes based on the two quantities u and t_1 agree well up to x near 3.1, further supporting the hypothesis of simple wavering behaviour, at which point they both break down (as can be foreseen from the profiles at $x = 3.5$ in figure 7). The dotted vertical lines beyond $x = 3.2$ result from large excursions of the apparent amplitudes after our definition $\tilde{y}' \equiv u'/|U_y|$ breaks down, and convey no information. The amplitudes are close to quadratic in x over $[2.2, 3.2]$ with an origin near $x = 1.8$. Their value at $x = 3.2$ is only 0.0016, which is indistinguishable in visualizations such as figure 1.

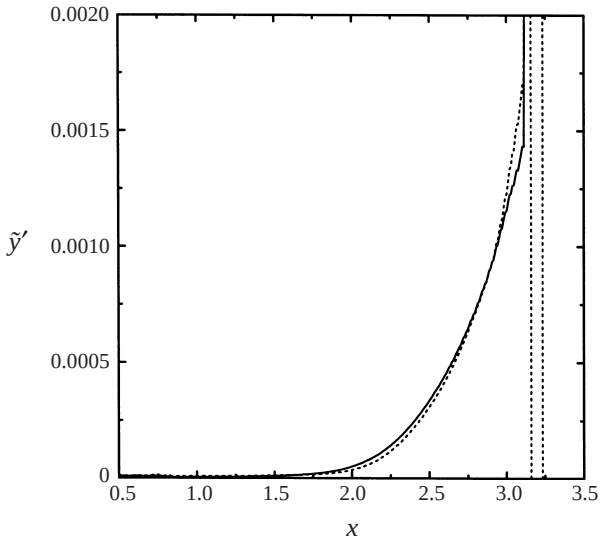

FIGURE 8. Waver amplitudes $\tilde{y}'$ deduced from the following fields: —, u; - - -, t_1.

4.4. *Late stages of transition and relaxation*

Having seen fine-scale turbulence in figure 1, we switch to the Reynolds-averaged description here. In figure 9 we show contours of the primary averaged quantities. The mean streamlines and the U and T contours exhibit the thin laminar detached shear layer, followed by a sudden widening as transition begins near $x = 3.5$. They are very reminiscent of Gaster's measurements (1966, figure 5). The peak negative mean velocity is -0.16, at $(x, y) = (3.75, 0.013)$. The concave streamline curvature, which we invoked earlier to explain the early pressure rise, is very noticeable near $x = 2.5$; the same applies near $x = 4.5$. The length of the bubble is 2, giving a Reynolds number of 66 000 based on the upstream velocity and 62 000 based on the edge velocity at separation (roughly 40 000 for the laminar part, and 22 000 after transition). This compares well with the value of 50 000 quoted by Lissaman (1983). The temperature and vorticity r.m.s. are confined to the boundary layer, but the velocity r.m.s. contains irrotational fluctuations and therefore extends much farther up. The temperature r.m.s. has a complex behaviour, quite unlike that of u', including a local minimum at $(x, y) = (3.75, 0.12)$ and high near-wall values. The double-peak behaviour is even more pronounced for t' than for u'. The non-zero values of t'_2 at the wall, especially between $x = 2.5$ and 3.5, will disappear at convergence.

The r.m.s. of vorticity (all three components added) rises to very high values near $x = 3.75$, as intense small-scale turbulence is generated; ω' then decays throughout the recovery region. We also show the pseudo shear stress $-\widetilde{u'v'} \equiv -\overline{u_i u_j} S_{ij} / \sqrt{2 S_{ij} S_{ij}}$, designed to equal the familiar $-\overline{u'v'}$ in parallel regions with $U_y > 0$, but to be insensitive to axis rotation. It can be viewed as the production of turbulent kinetic energy, normalized by the norm of the strain tensor. It takes very high values, near 0.02, at transition. These are even higher than for a mixing layer with the velocity difference that prevails at that station, namely $\Delta U \simeq 1.05$. Several authors have pointed out similarities between separated boundary layers and mixing layers (Driver 1991; Castro & Epik 1996). Over the recovery region, it decays dramatically to values near 0.0014, consistent with the skin friction ($C_f/2 \simeq 0.0013$). Small regions

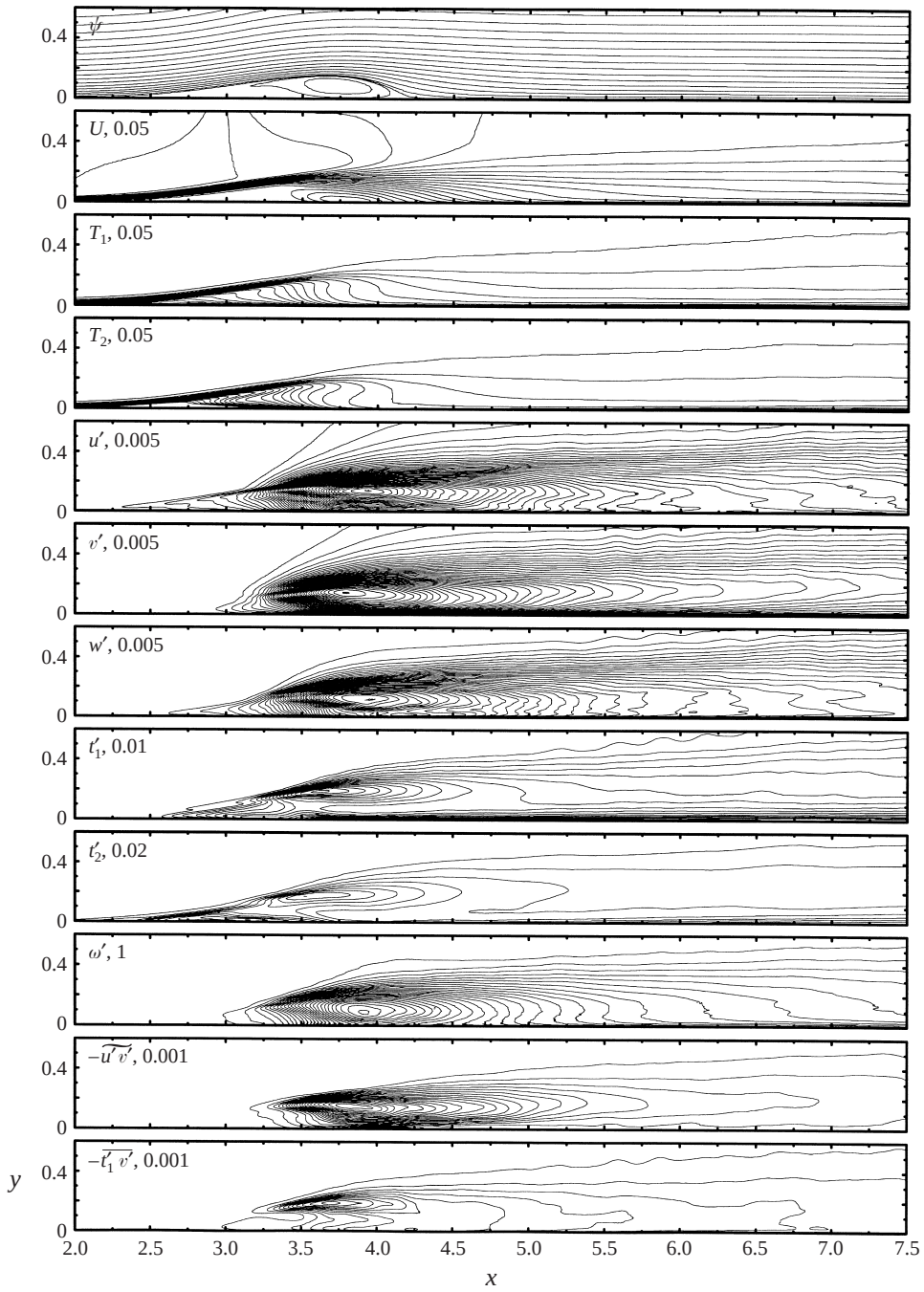

FIGURE 9. Contours of statistical quantities in the DNS. The variable and contour interval are given in each frame.

of negative production are found, particularly very near the wall at $x = 4$. Spalart & Coleman (1997) also found such regions, but had concerns that their flow might have unrealistic distortions; this is not the case here, as the size of the bubble closely approaches that in several experiments.

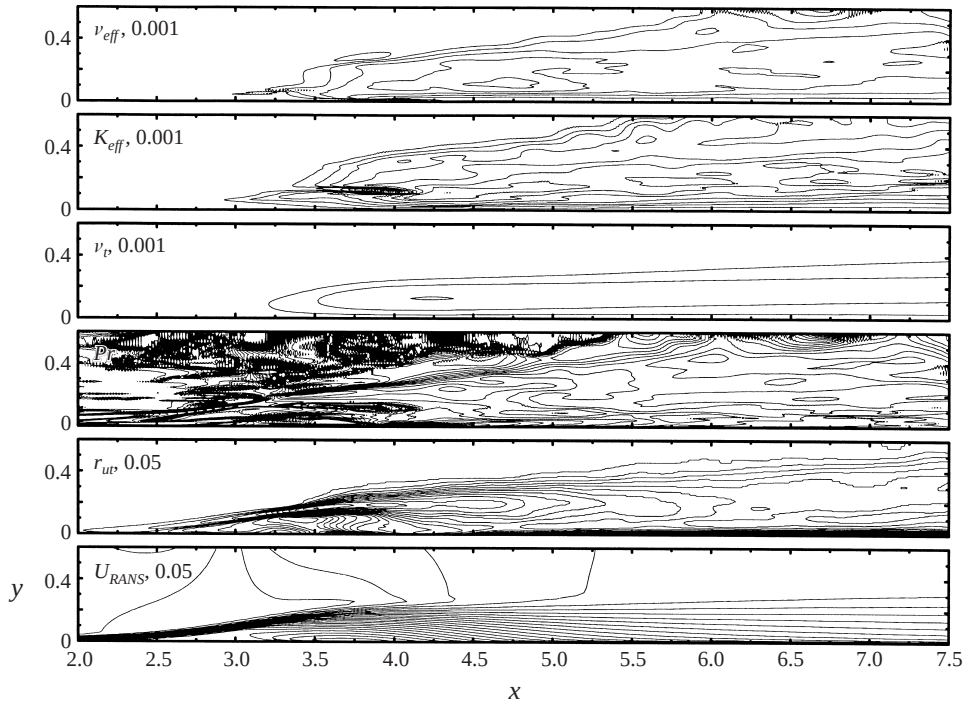

FIGURE 10. Contours of effective viscosity and diffusivity in the DNS; eddy viscosity the RANS; turbulent Prandtl number in the DNS; $u-t_1$ correlation coefficient in the DNS; and velocity in the RANS.

Finally, figure 10 compares the effective viscosity $\nu_{eff} \equiv -(\overline{u_i u_j} S_{ij})/(2S_{ij}S_{ij})$ of the DNS, defined in just the same spirit as the pseudo shear stress, the effective diffusivity $K_{eff} \equiv -(\overline{u_i t_1'} \partial T_1/\partial x_i)/(\partial T_1/\partial x_i \partial T_1/\partial x_i)$, and the actual eddy viscosity of the RANS. The agreement is quite poor even at the end of the useful region, as the peak value at $x = 7$ is about 0.003 in the DNS, but only about 0.0018 in the RANS. For a standard flat-plate boundary layer with this thickness, the peak value would be about 0.0013 for the S-A model, and near 0.001 for other mainstream turbulence models. Thus it appears that both DNS and RANS have elevated levels of turbulence, but that the relaxation is too rapid in the RANS. The effective Prandtl number K_{eff}/ν_{eff} may be too noisy to be very useful; it takes the expected values, somewhat below 1, in the well-behaved regions, and has large excursions of both signs in other regions. The RANS, of course, does not reproduce the negative values of the DNS effective viscosity and diffusivity, which represent counter-gradient diffusion in small regions (already seen in Spalart & Coleman 1997).

The next frame of the figure shows the correlation coefficient r_{ut} between u' and t_1'. boundary layer, again suggesting an incomplete relaxation. It then drops to essentially zero outside the turbulent region, as they found. Back near $x = 3.5$, the wavering shear layer contains positive values, without however reaching even 0.65. The correlation lingers near $+0.6$ at transition ($x \in [3.5, 4.5]$, $y \simeq 0.2$) and then steadily decays, while the near-wall values rise. Large negative values are found under the shear layer, peaking at about -0.35 at the point (3.45, 0.09) and exceeding -0.4 near the wall. The second temperature field gives very similar results. These results do not constitute an 'explanation' of the failure of the Reynolds analogy, but the description of such

excursions for a structural parameter of the turbulence could be of some use in turbulence-model development. The figure also suggests the variety of possible uses of the electronic dataset by colleagues.

The last frame of figure 10 may be compared with the second frame of figure 9. The differences in thickness are apparent.

5. Discussion

We have defined a problem of fluid mechanics which allows the detailed exploration of rich physics, and comparisons between various approaches. The geometry is simple, and three parameters fully define the velocity field. Connected work to date has been numerical, but we can hope for an experimental study. We conducted the DNS of the flow and offer it as the reference solution, pending a challenge from another DNS or an experiment, for physical description and for the assessment of RANS techniques. Another group is already engaged in such an effort, involving models much more elaborate than the ones we applied here (Hadzic & Hanjalić 1999).

The flow deserves interest because it contains laminar separation, a transition which we believe is independent of incoming disturbances, reattachment and some measure of relaxation. The Reynolds number, pressure distribution and structure of the separation bubble strongly evoke airfoils, although without their surface curvature, sweep, or compressibility. As often occurs, DNS allowed only one case to be run, but a few years will make more ambitious derivatives possible. We have two passive temperature fields with different wall boundary conditions, as a step in the direction of turbomachines.

The quantitative material consists primarily in distributions of pressure, skin friction, boundary-layer thicknesses, and heat-transfer rates, which are sufficient to challenge any turbulence model. The modelling situation regarding momentum transfer is acceptable, maybe surprisingly so. None of the turbulence models tested was designed to provide accuracy in transition, and the few models which have such features are designed to reproduce transition due to high free-stream turbulence, not transition due to back-flow. These results are reassuring for the use of simple transport models in complex flow fields with possible laminar patches (although it will be costly to provide a fine enough streamwise grid, without knowing the separation location in advance). Heat transfer is predicted much more poorly by RANS. A plausible reason is that the Reynolds analogy is distinctly violated by the DNS results. We note that an earlier fully-turbulent separation-bubble DNS had the same feature (Spalart & Coleman 1997), and it is tempting to attribute the loss of analogy partly to separation, and partly to transition. It remains to be seen how helpful this suggestion is for the improvement of RANS techniques.

The DNS also shows a slow relaxation, with very high turbulence levels relative to the friction velocity, and velocity profiles lower than normal in wall units.

The primary qualitative findings concern the transition mechanism. We convincingly discarded entry-region disturbances (necessarily, TS waves) as causes of the transition. Wavering of the thin separated shear layer was demonstrated, while the layer gradually escaped the confinement by the wall, thus increasing both its Kelvin–Helmholtz growth rates and its exposure to pressure signals from downstream. This brings it to a kind of critical condition, but the theory of absolute instability does not seem very helpful here. Transition is then sudden, not leaving time for vortex pairing, and apparently not analysable in terms of a primary, secondary, let alone tertiary instability. Three-dimensionality sets in very rapidly, and not in a manner suggestive

of a Görtler instability at all. The layer does have concave curvature at separation, but not near transition, and the total turning angle is a modest 7°. As a result, simulations with forced Görtler modes may be misguided; and stationary imperfections in an experiment may not be harmful.

Many extensions of this study are possible. The full relaxation to a simple zero-pressure-gradient turbulent boundary layer would make this a more complete test case, at a cost. Cases with intentional random inflow disturbances, higher than the residual disturbances here, would add evidence for the issue of whether this simulation depends on the inflow content. We could reduce the deceleration parameter S until transition fails to hold, and is evacuated downstream. This test might be very sensitive. We expect the threshold value to correspond with the threshold for flow reversal, but only roughly, and possibly with hysteresis if S is varied in time. Stability theory may be more successful there. Simulations with other ratios R_Y/R_X between channel depth and streamwise length would explore the effect of the opposite wall, which *is* a difference between this flow and airfoils. Cases with sweep would add realism for aerospace applications, and make a possible breakdown of the Reynolds analogy less predictable. We could also increase pressure gradient until the bubble bursts, but the number of grid points may well be prohibitive.

M. K. S was supported by the Boeing Technical Research Center in Moscow. The mainframe CPU time was donated by NAS. We greatly benefited from discussions with Drs J. D. Crouch, M. Alam, and B. van den Berg. The RANS calculations were done by Drs M. Shur and A. Travin, and part of the DNS by Dr G. Coleman. Dr G. Miller reviewed the manuscript.

REFERENCES

Alam, M. & Sandham, N. D. 1997*a* Simulation of laminar separation bubble instabilities. In *Direct and Large Eddy Simulation II* (ed. P. R. Voke, L. Kleiser & J. P. Chollet). Kluwer.

Alam, M. & Sandham, N. D. 1997*b* Numerical study of separation bubbles with turbulent re-attachment followed by boundary-layer relaxation. In *Parallel Computational Fluid Dynamics '97* (ed. A. Ecer, D. Emerson, J. Periaux & N. Satofuka). Elsevier.

Alving, A. E. & Fernholz, H. H. 1996 Turbulence measurements around a mild separation bubble and downstream of reattachment. *J. Fluid Mech.* **322**, 297.

Bell, D. M. & Ferziger, J. H. 1993 Turbulent boundary layer DNS with passive scalars. *Intl Conf. on Near-Wall Turbulent Flows, March 15–17, ASU, Tempe, AZ* (ed. R. M. C. So, C. G. Speziale & B. E. Launder), p. 327. Elsevier.

Bertolotti, F. P., Herbert, Th. & Spalart, P. R. 1992 Linear and nonlinear stability of the Blasius boundary layer. *J. Fluid Mech.* **242**, 441.

Castro, I. P. & Epik, E. 1996 Boundary-layer relaxation after a separated region. *Expl Therm. Fluid Sci.* **13**, 338.

Crouch, J. D. & Saric, W. S. 1986 Oscillating hot-wire measurements above an FX63-137 airfoil. *AIAA Paper* 86-0012.

Dianat, M. & Castro, I. P. 1991 Turbulence in a separated boundary layer *J. Fluid Mech.* **226**, 91.

Dovgal, A. V., Kozlov, V. V. & Michalke, A. 1994 Laminar boundary layer separation: instability and associated phenomena. *Prog. Aerospace Sci.* **30**, 61.

Driver, D. M. 1991 Reynolds shear stress measurements in a separated boundary layer flow. *AIAA Paper* 91-1787.

Gaster, M. 1966 The structure and behaviour of laminar separation bubbles. *AGARD CP* 4, pp. 813–854.

Hadzic, I. & Hanjalić, K. 1999 Modelling of separation-induced transition to turbulence with a second-moment closure. *4th Intl Symp. Eng. Turb. Modelling and Measurements, May 24–26, Corsica* (ed. W. Rodi & D. Laurence). Elsevier.

HORTON, H. P. 1967 A semi-empirical theory for the growth and bursting of laminar separation bubbles. *Aeronautical Research Council* CP1073.

HUERRE, P. & MONKEWITZ, P. A. 1985 Absolute and convective instabilities in free shear layers. *J. Fluid Mech.* **159**, 151.

LIEBECK, R. H. 1978 Design of subsonic airfoils for high lift. *J. Aircraft* **15**, 547.

LISSAMAN, P. B. S. 1983 Low-Reynolds-number airfoils. *Ann. Rev. Fluid Mech.* **15**, 223.

MAUCHER, U., RIST, U. & WAGNER, S. 1999 Transitional structures in a laminar separation bubble. *Proc. STAB-Symposium, Berlin, Nov. 10–12, 1998.* Notes on Num. Fluid Mech., Vieweg.

MAYLE, R. E. 1991 The role of laminar-turbulent transition in gas turbine engines. *J. Turbomachinery* **113**, 509.

MENTER, F. R. 1994*a* Two-equation eddy-viscosity turbulence models for engineering applications. *AIAA J.* **32**, 1598.

MENTER, F. R. 1994*b* A critical evaluation of promising eddy-viscosity turbulence models. *Intl Symp. on Turbulence, Heat and Mass Transfer. Lisbon, Aug. 9–12, 1994.*

MICHALKE, A. 1965 On spatially growing disturbances in an inviscid shear layer. *J. Fluid Mech.* **23**, 521.

PAULEY, L. L., MOIN, P. & REYNOLDS, W. C. 1990 The structure of two-dimensional separation. *J. Fluid Mech.* **220**, 397.

RIPLEY, M. D. & PAULEY, L. L. 1993 The unsteady structure of two-dimensional steady separation. *Phys. Fluids* A **5**, 3099.

RIVIR, R. B., JOHNSTON, J. P. & EATON, J. K. 1994 Heat transfer on a flat surface under a region of turbulent separation. *J. Turbomachinery* **116**, 57.

ROGERS, S. E. & KWAK, D. 1990 Upwind difference scheme for the time-accurate incompressible Navier–Stokes equations. *AIAA J.* **28**, 253.

SHUR, M., STRELETS, M., ZAIKOV, L., GULYAEV, A., KOZLOV, V. & SECUNDOV, A. 1995 Comparative numerical testing of one- and two-equation turbulence models for flows with separation and reattachment. *AIAA Paper* 95-0863.

SHUR, M. L., SPALART, P. R., STRELETS, M. KH. & TRAVIN, A. K. 1996 Navier–Stokes simulation of shedding turbulent flow past a circular cylinder a cylinder with a backward splitter plate. *Third Eur. CFD Conf., Paris.*

SPALART, P. R. 1988*a* Direct numerical study of leading-edge contamination. *AGARD CP*-438.

SPALART, P. R. 1988*b* Direct simulation of a turbulent boundary layer up to $R_\theta = 1410$. *J. Fluid Mech.* **187**, 61.

SPALART, P. R. & ALLMARAS, S. R. 1994 A one-equation turbulence model for aerodynamic flows. *Rech. Aérosp.* **1**, 5.

SPALART, P. R. & COLEMAN, G. N. 1997 Numerical study of a separation bubble with heat transfer. *Eur. J. Mech.* B **16**, 2.

SPALART, P. R. & STRELETS, M. KH. 1997 Direct and Reynolds-averaged numerical simulations of a transitional separation bubble. *11th Symp. on Turb. Shear Flows. Sept. 8–10, Grenoble, France* (ed. M. Lesieur, B. E. Launder, G. Binder & J. H. Whitelaw).

VAN DYKE, M. 1982 *An Album of Fluid Motion.* Parabolic Press, Stanford, CA, USA.

VOGEL, J. C. & EATON, J. K. 1985 Combined heat transfer and fluid dynamic measurements downstream of a backward-facing step. *J. Heat Transfer* **107**, 922.

WILSON, P. G. & PAULEY, L. L. 1995 Large eddy simulation of a transitional separation bubble. *10th Symp. on Turb. Shear Flows, Aug. 14–16, Univ. Park, PA.* Also *Phys. Fluids* **10**, 2933.

YANG, Z. & VOKE, P. R. 1995 Large-eddy simulation of boundary layer transition on a flat plate with semi-circular leading edge. *10th Symp. on Turb. Shear Flows. Aug. 14–16, Univ. Park, PA.*